CFD-ASSISTED OPTIMISATION OF THE NITRATOR DESIGN FOR MILITARY PROPELLANT PRODUCTION

JIMMY LEA AND ADESOJI A. ADESINA*

Abstract - The manufacture of nitrocellulose, which is the basis of most artillery, tank, mortar and rocket propellant is intrinsically risky due to the energetic nature of the product and the sensitivity of the process. To optimise the performance of the nitrator, computational fluid dynamics (CFD) technology was employed to initially select a suitable impeller design and subsequently used to select an appropriate nitrator geometrical configuration. From the qualitative and quantitative analysis, a baffled-nitrator was proposed. The results obtained on the proposed nitrator were compared to those obtained from the existing unbaffled-nitrator and the comparison indicated that the proposed nitrator performed more effectively relative to the existing nitrator.

I. Introduction

In the Commonwealth of Australia – owned munition plant, mixed acids consisting of 61% concentrated nitric acid (HNO_3), 29% concentrated sulphuric acid (H_2SO_4) and 10% H_2O are used to nitrate the alpha cellulose boards (ACB) to nitrocellulose. Nitrocellulose is a highly flammable energetic compound manufactured by reaction of ACB with HNO_3, in the presence of H_2SO_4. It is represented by:

$$C_6H_{10}O_5 + xHNO_3 \Leftrightarrow C_6H_{10-x}O_{5-x}(ONO_2)_x + xH_2O$$

This reaction process adds a large amount of O_2 to the chemical structure of the cellulose. To enhance the rate of reaction, it is essential that any mass transfer limitation be eliminated or minimised. For any reaction to take place, mass transfer from the bulk liquid to the immediate region surrounding the ACB particles must take place. The fluid surrounding the particles will react with the ACB and be depleted. To ensure a continuous high reaction rate is maintained, the depleted mixed acids must be replaced with fresh acid from the bulk fluid.

The authors are with:
Reactor Engineering and Technology Group
School of Chemical Sciences and Engineering,
The University of New South Wales, NSW 2052, Australia
* Corresponding author: a.adesina@unsw.edu.au

Thus, an obvious way to maintain a high reaction rate is to increase the relative velocity between the mixed acids and the ACB particles. This can be achieved by investigating ways to induce high turbulence without compromising on other aspects of this reaction.The objective of this paper is to optimise this nitrator via CFD modelling and simulation. This is achieved by conducting simulations on a proposed system and the results were benchmarked against those obtained from the existing system. Detailed CFD modelling and simulation on the existing system can be found in Lea & Adesina [1].

The nitrator of interest, shown in Fig. 1 (left), is responsible for the production of military propellant. Its geometrical configuration consists of a set of impellers mounted on a top-entry shaft, rotating at 73 rpm under normal operating condition. The 676L-nitrator is unbaffled and unjacketed.

Fig. 1. Nitrator of interest (left)

ISBN:978-988-98671-2-6

II. Theoretical Consideration

A. Numerical setup

Fluent® 6.2 solver was used to create a numerical solution that matches the governing conservation equations. In this study, the focus was on solving the conservation of mass, momentum, turbulence transport and volume fraction with a view to generating a steady-state 3D hydrodynamics profile and transient results.

In this work, the solution domain was restricted to the tanks and that flow within the feed pipes was not modelled. To simulate impeller rotations, separate rotational zones in the immediate vicinity of the impellers were created and a multiple reference frame (MRF) approach was used. This method involved solving the flow characteristics of the inner region using a rotating framework. These results were then used to provide boundary conditions for the outer region which employed a stationary framework to secure solution to the flow characteristics. The results from the outer region were then re-supplied as boundary conditions for the inner region. This iterative procedure was repeatedly performed until a convergent solution was obtained for both regions.

The segregated-implicit method, where the governing equations were solved sequentially was used. To obtain a higher degree of accuracy, all solutions were obtained via the second-order upwind scheme. Due to the absence of baffles, significant uninterrupted rotational flow existed inside the nitrator.

However, in the baffled-tank with highly interrupted rotational flow, a steep pressure gradient exists. As a result, PRESTO (pressure staggering option) was employed to compute the pressure value at the cell surface by interpolating the value at cell centroid. SIMPLE (semi-implicit method for pressure linked equations) scheme was used for the pressure velocity coupling where a relationship between the pressure and velocity corrections was used to enforce conservation of continuity in order to obtain the pressure field.

To simulate the air draw-down, the multiphase model using volume of fluid (VOF) approach was employed. This model was designed for two or more immiscible fluids where the position of the interface between the fluids is of interest and depends on the fact that the air and fluid are not interpenetrating. Each phase is represented by its volume fraction therefore in each control volume the volume fraction representing air and the fluid phase equals to unity. Moreover, the fields for all variables and properties are shared by the phases and represent volume-averaged values. This is valid only if the volume fraction of each of the phases is known at each location. This means that the variables and properties in any given cell either purely represents one of the phases or represents a mixture of the phases, depending upon the volume fraction values.

To speed up the iteration process, a convergence acceleration technique called full multigrid method (FMG) was employed where the multigrid process starts on a coarse grid, carries out a number of cycles and then transfers the solution to a finer grid, where the multigrid cycles are performed again. The procedure is then successively repeated until the finest grid is reached. Since FMG initialisation does most of the work on coarse levels, this initialisation procedure is computationally inexpensive and, for large problems, a good initial solution can be obtained in a fraction of the time spent to converge on a final solution.

Simulations were generally considered converged when the residuals for mass, momentum and turbulence transport and volumetric fraction fell below 1×10^{-4}. Further checks for convergence were made by creating a monitoring point inside the tank and ensuring that the value monitored remained constant with repeated iterations.

III. Impeller Selection

Before designing an effective nitrator, a suitable impeller must be selected. Six different impeller designs were modelled and simulated to determine their suitability for the nitrator in question. Table 1 summarises the results obtained.

Table 1. Results of various impeller designs

Impeller	P (W)	T (Nm)	Q (kg s^{-1})	N_P	N_Q	η
HE-4	85.51	8.165	49.63	0.6056	0.1883	0.3110
ADI-HE	68.63	6.554	44.48	0.4860	0.1688	0.3473
PBT	118.5	11.32	44.75	0.8392	0.1698	0.2024
Paddle	178.3	17.03	7.69	1.263	0.0292	0.0231
30° – 4 blades	84.47	8.067	43.58	0.5982	0.1654	0.2764
30° – bended blades	68.73	6.563	44.71	0.4868	0.1697	0.3486

Judging from the results tabulated, the paddle impeller produced low axial flow (Q) and at the same time, promotes high radial flow. Apart from having high power consumption, the paddle impeller will not create turbulence, instead, will promote 'laminar' like rotational flow. Its low axial flow and high power consumption contributed to its very low efficiency relative to the other impellers. Based on this, the paddle impeller was excluded.

The other five impellers have comparable performance based on their respective efficiency values. The most notable impellers were the ADI-HE and the 30°-bendedblades where their performance matches each other. These two were short listed and decision to select one between them depended on qualitative analysis. Although the 30°-bendedblades has similar performance with the two short listed impellers, its performance was much lower under baffled setting. This was attributed to the shallow angle of attack which promoted axial flow and minimum radial flow.

For baffle to work well, a fair amount of radial flow component must exist.

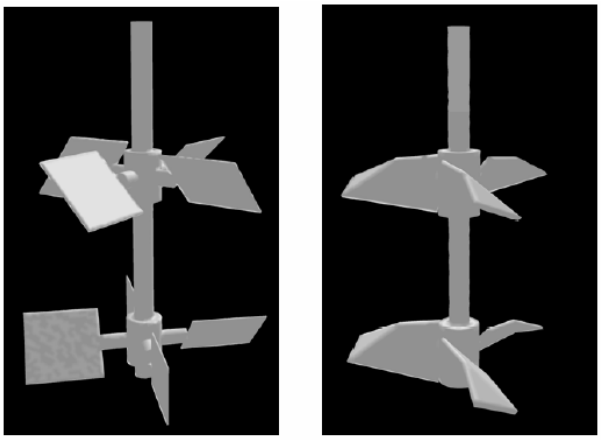

Fig. 2. Existing impellers (left) and proposed impellers (right)

Fig. 2 shows the existing 4-bladed impellers setup which will be replaced by the proposed 3-bladed high-efficiency impeller setup.

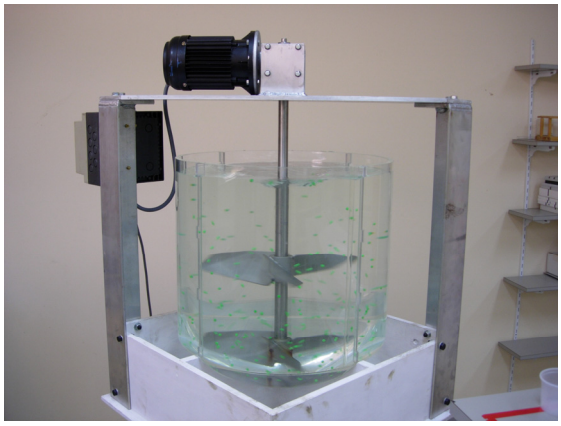

Fig. 3. Pilot-scale nitrator

Fig. 3 shows a 100L pilot-scale nitrator fabricated to determine the effectiveness of the selected geometrical configuration to suspend and draw down particles. The test showed that this configuration was effective in suspending and drawing down floating solids.

IV. Nitrator Geometry Selection

A. Nitrator selection

Table 2 shows eight nitrator geometrical configurations under investigation. Fig. 4 shows the diagrammatic representation of each of these variants.

Table 2. Factorial-experiment trial condition

Variant #	1	2	3	4	5	6	7	8
No. of baffles	2	2	2	2	4	4	4	4
Impeller diameter	0.55T	0.55T	0.6T	0.6T	0.55T	0.55T	0.6T	0.6T
No. of impellers	1	2	1	2	1	2	1	2
Blade width	0.3D	0.35D	0.35D	0.3D	0.35D	0.3D	0.3D	0.35D

MixSim® 2.0 was used to build the geometry and mesh the nitrator configurations. For baffled system, unstructured mesh consisting of mainly tetrahedral cells was employed which were good enough to ensure solution convergence and to obtain highly accurate results.

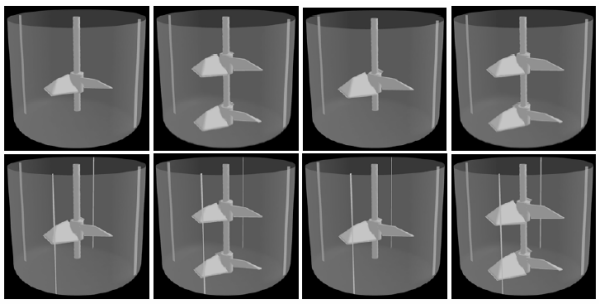

Fig. 4. Various nitrator geometrical configurations

Table 3. Results of various nitrator configurations

Variant #	1	2	3	4	5	6	7	8
τ	10.86	17.41	16.99	22.5	12.38	16.74	16.85	26.82
Q	93.61	155.3	107.5	171.6	126	209.1	139.3	246.6
N	1.217	1.217	1.217	1.217	1.217	1.217	1.217	1.217
P	83.03	133.1	129.9	172.0	94.65	128	128.8	205.1
D	0.55	0.55	0.60	0.60	0.55	0.55	0.60	0.60
ρ	1713	1713	1713	1713	1713	1713	1713	1713
N_P	0.5348	0.8573	0.5415	0.7171	0.6096	0.8243	0.5370	0.8547
N_Q	0.2700	0.4479	0.2388	0.3812	0.3634	0.6030	0.3094	0.5478
η	0.5048	0.5244	0.4410	0.5316	0.5961	0.7316	0.5762	0.6409

Table 3 shows the results of each nitrator configuration. Of these eight variants, variant 6, shown in Fig 5., was chosen as the desired design. To ensure that the results were not influenced by the number of cells, grid independence test was conducted.

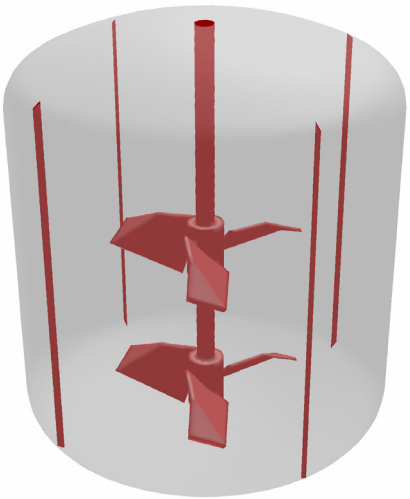

Fig. 5. Meshed nitrator

B. *Grid independence*

A preliminary grid convergence study was carried out on variant 6 to verify that the solution obtained from using the second-order upwind discretisation scheme was mesh independent. The number of cells inside and outside the rotational zones was systematically increased in the x-, y- and z-directions throughout the tank. When refining the mesh, care was taken to assign additional cells to the regions of high gradient around the impeller blades and discharge regions. Simulation results did not show significant changes (<1%) when the number of cells was increased.

V. Comparison of Systems

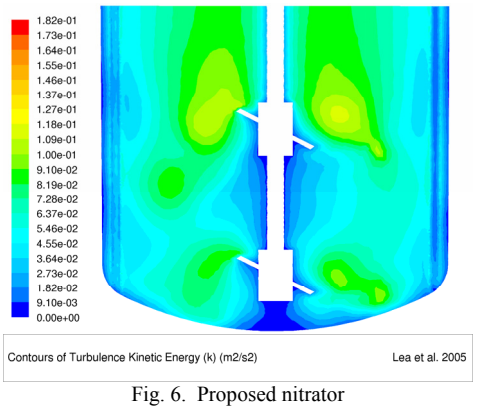

Fig. 6. Proposed nitrator

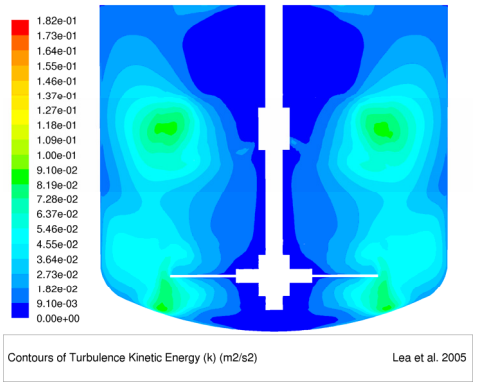

Fig. 7. Existing nitrator

Figs. 6 and 7 represent the contours of turbulence kinetic energy of the proposed and the existing nitrators respectively. They show that in both systems the lowest turbulence areas are confined to those above the impellers, around the shaft and at the tank bottom. In the proposed system, the areas of low turbulence present in the existing system vanished and the low turbulence region at the tank bottom was significantly minimised. Moreover, turbulence around wall region in the proposed system is higher relative to the existing system.

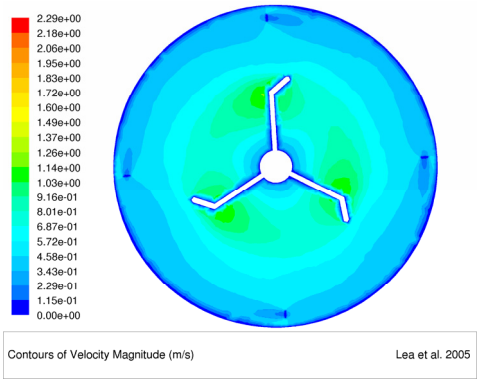

Fig. 8. Proposed nitrator

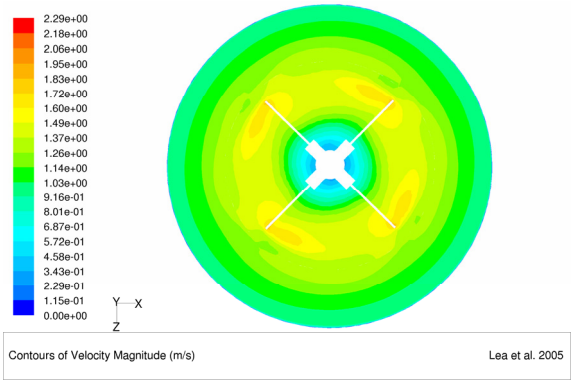

Fig. 9. Existing nitrator

The contours of velocity magnitude of the proposed nitrator in Fig. 8 shows that the velocity magnitude is lower, relative to the existing system, shown in Fig. 9. In the proposed system, the fastest region is located around impeller region and fades with distant from the impeller. A thin layer of very low velocity can be found along the wall, due to boundary layer effect. The lower overall velocity magnitude can be attributed to the conversion of the power dissipated from the impellers to creating turbulence in the nitrator.

Table 4. Comparison of existing and proposed systems

Parameter	Existing	Proposed	Impv, %
Power number, N_P	0.6089	0.8243	35.38
Flow number, N_Q	0.2615	0.6030	130.6
Flow efficiency, η	0.4295	0.7316	70.34
Flowrate, kgs^{-1}	117.8	209.1	77.50
Blending time, t_B, s	26.82	15.68	41.54
Deviation from ideality, ξ, %	14.13	4.53	67.92
Global turbulence, $m^2 s^{-2}$	37,014	51,535	39.23

Table 5 above shows the power number ($P/[\rho \times N^3 \times D^5]$) increases by 35.38% which can be attributed to the installation of four narrow baffles. Although it is desirable to minimise power consumption, in some cases, more power is required to achieve process objective. In this case, a higher power consumed means more power is delivered into the process fluid.

The flow number ($Q/[\rho \times N \times D^3]$) has been increased to 130.6% at the same rotational speed and using a slightly smaller diameter impeller. The huge increase is attributed to the new impeller design and the installation of four narrow baffles which promoted axial flow.

Flow efficiency [$(N_Q/N_P) \times 100\%$] which increased by 70.34%, shows that the proposed system is much more power efficient than the existing system. Since the draw-down of floating particles can be achieved via two mechanisms, that is, the intensity of turbulence and the formation of surface vortex. In this case, since the formation of surface vortex was suppressed by four narrow baffles, power consumption, position of the impeller with respect to the free surface, and type of impeller (axial/radial) becomes the controlling parameters, which means that high liquid velocity and the intensity of the turbulence are responsible for pulling down the buoyant solids. The proposed system has velocity 77.50% higher than that of the existing system coupled with a higher global turbulence.

High flowrate will help to promote the draw-down of floating ACB. Blending time was shortened by 41.54% which can be translated into a higher plant throughput. Deviation from ideality was reduced by 67.92% which mean the room for improving the blending time is now much smaller. Finally, the global turbulence for the proposed system exceeded that of the existing system by 39.23%, thus the mass transfer rate should increase significantly.

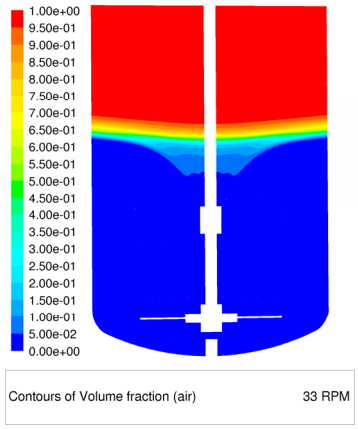

Fig. 10. Contours of air volume fraction – top view

Fig. 10 shows the result derived from a multiphase modelling using VOF approach. The aim of this modelling is to snapshot the air draw-down occurring in the nitrator during start-up and steady-state operation; and subsequently to convey this snapshot in the form of the contours of air volume fraction. As shown in the contours plot, the central vortex is already prevalent even when the impellers are rotating at 33 rpm. This phenomenon is attributed to the absence of baffles that reduce bulk fluid rotation inside the nitrator.

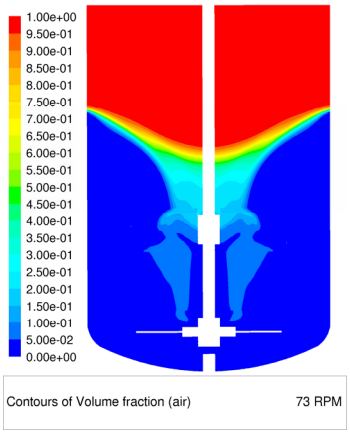

Fig. 11. Contours of air volume fraction – top view

The central vortex deepened as the speed was increased to 73 rpm, as shown in Fig 11. Air entrainment, defined as the situation where the air pocket hits the impeller hub, partly occurred even at 73 rpm. In the absence of baffles, the vortex formed will promote the draw-down of floating solids, however, the floating solids have the tendency of concentrating in the central vortex which leads to its poor distribution throughout the nitrator. The concentration of floating solids will eventually leads to a significant reduction in mass transfer thus lowering reaction rate.

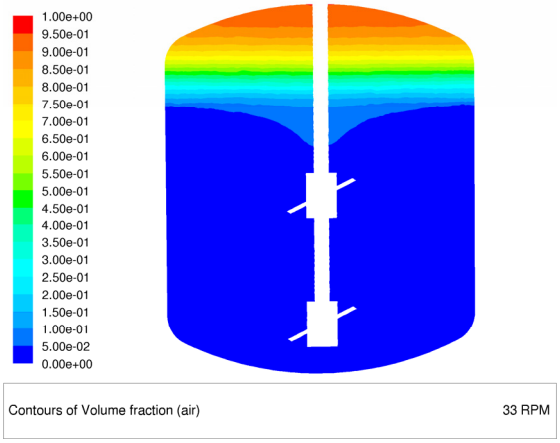

Fig. 12. Meshed nitrator

Fig. 12 shows that at 33 rpm, 10% of air reaches halfway through between the top impeller and the free surface. There was not the slightest vortex on the free surface.

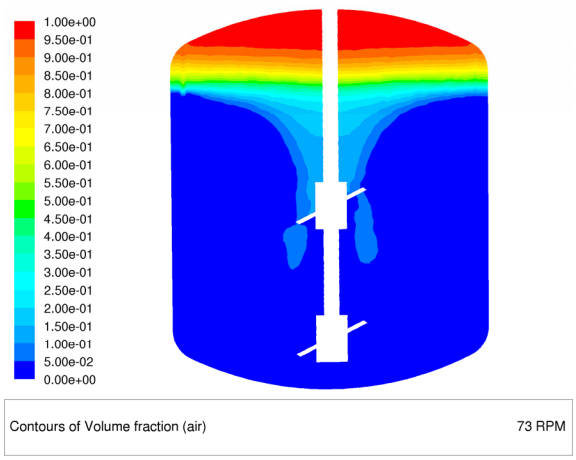

Fig. 13. Meshed nitrator

Fig. 13 shows that at 73 rpm, the vortex becomes deeper and slightly exceeded the top impeller hub. A comparison of the percentage air drawn-down was presented in Table 6. It shows that air-entrainment of the existing nitrator exceeded that of the proposed nitrator at all the speeds simulated.

Table 5. Comparison of existing and proposed systems

Impeller speed	Existing (%)	Proposed (%)
33	2.50	2.55
53	2.50	7.0
73	17.5	12.44
93	32.5	17.19
113	57.5	20.69
133	62.5	25.68

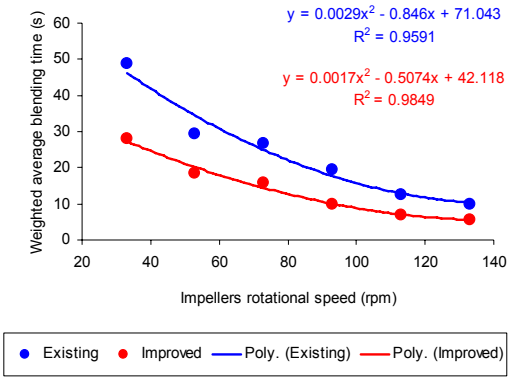

Fig. 14. Meshed nitrator

Fig. 14 shows the plot of weighted average blending time versus various impeller speeds, for both the existing and proposed nitrators. It can be seen that in both cases, when the impellers rotational speed increases, the weighted average blending time decreases almost monotonically. This correlation will make it easier to predict the minimum time required to achieve a specified level of homogeneity if the impeller speed were to change. The plot clearly shows that the proposed nitrator has a significant blending time reduction starting from 33 rpm to 133 rpm. The gap of improvement became narrower as the impeller speed was increased.

VI. Conclusions

In this study, CFD was employed to optimise the nitrator used in the manufacture of military propellants. Quantitatively, the power number, flow number, flow efficiency, blending time and deviation from ideality for the new design are better than those for the existing system. It is also evident that the proposed nitrator design will also enhance mass transfer.

Acknowledgements

The authors are grateful to Paul Flavel, manufacturing operations manager of Thales Australia's munitions plant, for his sponsorship of this process R&D project.

Reference

1. Lea and Adesina [2007], A numerical-based characterisation of the nitrator utilised in the manufacture of military propellant, ICAEM'07, London, United Kingdom